

Energy-Resolved Information Scrambling in Energy-Space Lattices

S. Pegahan¹, I. Arakelyan, and J. E. Thomas^{1*}

Department of Physics, North Carolina State University, Raleigh, North Carolina 27695, USA

 (Received 4 September 2020; revised 10 December 2020; accepted 28 January 2021; published 19 February 2021)

Weakly interacting Fermi gases simulate spin lattices in energy space, offering a rich platform for investigating information spreading and spin coherence in a large many-body quantum system. We show that the collective spin vector can be determined as a function of energy from the measured spin density, enabling general energy-space resolved protocols. We measure an out-of-time-order correlation function in this system and observe the energy dependence of the many-body coherence.

DOI: [10.1103/PhysRevLett.126.070601](https://doi.org/10.1103/PhysRevLett.126.070601)

Trapped, weakly interacting Fermi gases provide a new paradigm for the study of many-body physics in a large quantum system containing $N \simeq 10^5$ atoms with a tunable, reversible Hamiltonian [1,2]. In this system, coherent superpositions of two hyperfine states behave as pseudo-spins and the s -wave scattering length is magnetically tuned to nearly vanish [1,3,4]. The corresponding collision rate is negligible, so that single atom energies are conserved [1,5–7] over the experimental timescale. The conserved single particle energy states label the “sites” of an effective energy-space lattice, simulating a variety of spin-lattice models [8]. Interactions are effectively long range in energy space [4,8,9], important for new studies of information scrambling in a far from equilibrium, nearly zero temperature regime [10] and for applications to fast scrambling [11] and “out-of-equilibrium” dynamics in spin-lattice systems [12]. However, measurements in weakly interacting Fermi gases [1–7] have been limited to the spatial profiles of the collective spin density or the total number of atoms in each spin state, precluding observation of many-body correlations in chosen sectors of the energy-space lattice.

Of particular interest is the measurement of out-of-time-order correlation (OTOC) functions in weakly interacting Fermi gases. Certain OTOC functions [13–16] can serve as entanglement witnesses and to quantify coherence and information scrambling in quantum many-body systems [10,17]. Originally, OTOC measurements were performed by reversing the time evolution of the many-body state in nuclear magnetic resonance experiments at high temperatures, where the initial state is described by a density operator and high order quantum coherence was observed [18]. New OTOC studies have been done in trapped ion systems containing relatively small numbers of atoms, where the individual sites are nearly equivalent, and the initial state is pure [10]. Related methods have been developed for systems containing up to 100 atoms [19], but the application of OTOC measurement to trapped ultracold gases has remained a challenge.

In this Letter, we report the demonstration of a general method for performing energy-resolved measurements of the collective spin vector in a harmonically trapped weakly interacting Fermi gas. We show that OTOC measurements can be implemented in this system and we extract many-body coherence in energy-resolved sectors, paving the way for new protocols, such as time-dependent energy-space correlation measurements.

In the experiments [20], we begin with a degenerate cloud of ${}^6\text{Li}$ containing a total of $N = 6.5 \times 10^4$ atoms in a single spin state. The cloud is confined in a harmonic, cigar-shaped optical trap, with oscillation frequencies $\omega_x/2\pi = 23$ Hz along the cigar x axis and $\omega_r/2\pi = 625$ Hz in the transverse (y, z) directions. The corresponding Fermi temperature $T_F = 0.73$ μK and $T/T_F = 0.32$.

We employ the two lowest hyperfine-Zeeman states, which are denoted by $|1\rangle \equiv |\uparrow_z\rangle$ and $|2\rangle \equiv |\downarrow_z\rangle$. The cloud is initially prepared in state $|\downarrow_z\rangle$ in a bias magnetic field of 528.53 G, where the s -wave scattering length $a_{12} \equiv a = 4.24a_0$ [4]. In this case, the largest possible collision rate γ_c in the Fermi gas arises for an incoherent mixture with $N/2$ atoms in each of two spin states. We find $\gamma_c < 1.7 \times 10^{-3} \text{ s}^{-1}$ [21], which is negligible for the experimental timescale < 1 s. Hence, the single particle energies are conserved and the energy distribution is time independent, as observed in the experiments [4,20].

The Hamiltonian for the confined weakly interacting Fermi gas can be approximated as a one-dimensional (1D) spin “lattice” in energy space [4],

$$H(a) = a \sum_{i,j \neq i} g_{ij} \mathbf{s}_i \cdot \mathbf{s}_j - \sum_i \Omega_i s_{zi}, \quad (1)$$

where we take $\hbar \equiv 1$. We associate a “site” i with the energy $E_i = (n_i + 1/2)\hbar\nu_x$ of an atom in the i th harmonic oscillator state along the cigar axis x . For each E_i , we define a dimensionless collective spin vector $\mathbf{s}_i = \sum_{\alpha_i} \mathbf{s}_{\alpha_i}$, where the sum over α_i includes the occupied transverse (n_y, n_z)

states for fixed n_i . As $k_B T_F / \hbar \omega_x \simeq 650$, the average number of atoms at each site is $N/650 \simeq 100$ [22].

The first term in Eq. (1) is a site-to-site interaction, proportional to the s -wave scattering length a and to the overlap of the harmonic oscillator probability densities for colliding atoms, $g_{ij} \propto \int dx |\phi_{E_i}(x)|^2 |\phi_{E_j}(x)|^2 \propto 1/\sqrt{|E_i - E_j|}$, which is an effective long-range interaction in the energy lattice [4]. For a zero temperature Fermi gas, the average interaction energy is $a\bar{g} = 3.8\Omega_{\text{MF}}$ [23], where the mean-field frequency [4] for our experimental parameters is $\Omega_{\text{MF}}/2\pi \simeq 0.5$ Hz, i.e., $a\bar{g}/2\pi \simeq 1.9$ Hz.

The second term in Eq. (1) is an effective site-dependent Zeeman energy, arising from the quadratic spatial variation of the bias magnetic field along x , which produces a spin-dependent harmonic potential. As $\omega_r/\omega_x = 27$, the corresponding effect on the transverse (y, z) motion is negligible, so that all atoms at site i have the same Zeeman energy. In Eq. (1), $\Omega(E_i) \equiv \Omega_i = \Omega' E_i + \Delta'$, where $\Omega' = -\delta\omega_x/\hbar\omega_x$, with $\delta\omega_x/2\pi = 14.9$ mHz for our trap [4]. For atoms with the mean energy $\bar{E}_x \simeq k_B T_F/4$, $\Omega' \bar{E}_x/2\pi \simeq 2$ Hz. We define $\Delta' \equiv \Delta - \Omega' \bar{E}_x$, where Δ is the global detuning and $\Delta = 0$ corresponds to $\Omega_i = 0$ for the mean energy, $E_i = \bar{E}_x$.

A key feature of our experiments is the extraction of energy-resolved spin densities $n_{\uparrow_z, \downarrow_z}(E)$ by inverse-Abel transformation of the corresponding 1D spatial profiles $n_{\uparrow_z, \downarrow_z}(x)$, which are obtained from absorption images of a single cloud. The transform method requires a continuum approximation, which is justified for the x direction, where $k_B T_F / \hbar \omega_x = 650$. Further, we require negligible energy space coherence; i.e., the atomic spins remain effectively localized in their individual energy sites. This assumption is justified by the very small transition matrix elements $< 10^{-4} \hbar \omega_x$ [24] between three-dimensional harmonic oscillator states, which arise from short-range interactions between two atoms [20].

In this regime, the spatial profile for each spin state $n_\sigma(x)$, $\sigma \equiv \uparrow_z, \downarrow_z$, is an Abel transform of the corresponding energy profile $n_\sigma(E)$ [20]:

$$n_\sigma(x) = \int dE |\phi_E(x)|^2 n_\sigma(E) = \frac{\omega_x}{\pi} \int_0^\infty dp_x n_\sigma \left(\frac{p_x^2}{2m} + \frac{m\omega_x^2}{2} x^2 \right). \quad (2)$$

In Eq. (2), the last form is obtained by using a WKB approximation for the harmonic oscillator states $\phi_E(x)$ [20]. An inverse-Abel transform [20,25] of $n_\sigma(x)$ then determines $n_\sigma(E)$ with a resolution $\Delta E \simeq 0.04 E_F$ [20].

For the protocol of Fig. 1(a), discussed in detail below, Fig. 1(b) shows the measured *single-shot* spin density, $S_z(x, \phi) = [n_{\uparrow_z}(x, \phi) - n_{\downarrow_z}(x, \phi)]/2$, in units of the central total spin density $n(0)$. Figure 1(c) shows the corresponding single-shot $S_z(E, \phi)$, obtained by inverse-Abel transformation of $S_z(x, \phi)$. We see that $S_z(E, \phi)$ appears smooth compared to the single-shot spin density $S_z(x, \phi)$, which requires averaging over several shots to obtain a smooth profile. To check that the inverse-Abel transform has adequate energy resolution, we Abel transform the extracted $S_z(E, \phi)$, yielding the red dotted curve of Fig. 1(b), which is consistent with the measured density profile [20].

Our experimental OTOC protocol, Fig. 1(a), applies a rotation ϕ to the total interacting spin system in between forward and time-reversed evolutions. Then, a measurement of s_{zi} is performed to diagnose the effects of the rotation on the spins at “site i ” in energy space. We start by preparing a fully z -polarized state $|\downarrow_{z1}\downarrow_{z2}\dots\downarrow_{zN}\rangle \equiv |\psi_{z0}\rangle$ in a bias magnetic field $B_1 = 528.53$ G, where the scattering length $a_1 \equiv a = 4.24a_0$. Then we apply a 0.5 ms radio-frequency $(\pi/2)_y$ pulse (defined to be about the y axis), which is resonant with the $|\downarrow_z\rangle \rightarrow |\uparrow_z\rangle$ transition at the bias field B_1 , to produce an initial x -polarized N -atom state $|\psi_0\rangle = e^{-i(\pi/2)S_y} |\psi_{z0}\rangle = |\uparrow_{x1}\uparrow_{x2}\dots\uparrow_{xN}\rangle$. The system evolves for a time $\tau = 200$ ms at the initial bias magnetic field $B_1 = 528.53$ G. Then, a resonant radio-frequency pulse $(\phi)_x$, shifted in phase from the first pulse by $\pi/2$, rotates the N -atom state about the x axis [26] by a chosen angle ϕ . Immediately following this rotation, we

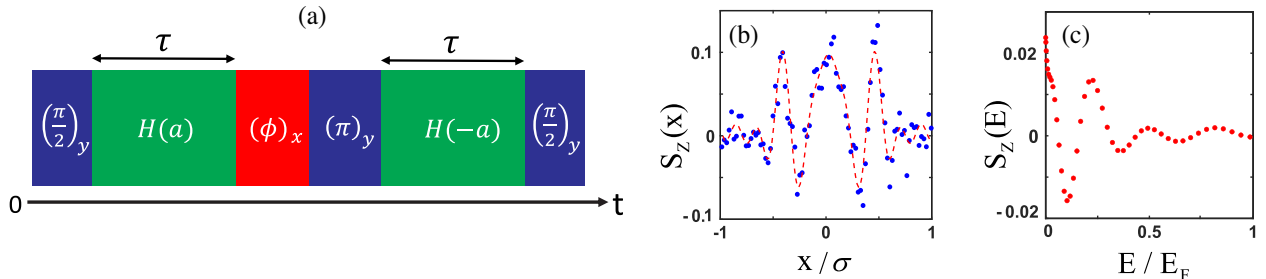


FIG. 1. Energy-resolved out-of-time-order correlation (OTOC) measurement. The system is initially prepared in a pure state, with the spins for atoms of energy E_1, E_2, \dots, E_N polarized along the $-z$ axis. (a) OTOC sequence, after which the spatial profiles of the \uparrow_z and \downarrow_z states are measured for each cloud by resonant absorption imaging. (b) “Single-shot” spin density profile $S_z(x)$ (blue dots). For this measurement, the scattering length in the Hamiltonian $H(a)$ is $a = 4.24a_0$, $\phi = \pi$, and $\sigma = 345 \mu\text{m}$. (c) An inverse-Abel transform of the spatial profile (blue dots) extracts the single-shot energy-resolved spin density $S_z(E)$ (red dots). An Abel transform of $S_z(E)$ yields the red dashed curve shown in (b), consistent with the data.

reverse the sign of the Hamiltonian by applying a $(\pi)_y$ pulse and tuning the bias magnetic field to a value $B_2 = 525.83$ G, where the scattering length $a_2 = -a$, i.e., $e^{i\pi S_y} H(-a) e^{-i\pi S_y} = -H(a)$, from Eq. (1). After the system evolves for an additional time τ , the bias field is ramped back to B_1 , and a final $(\pi/2)_y$ pulse is applied [20]. The final state of the N -atom system after the pulse sequence of Fig. 1(a) can be written as

$$|\psi_f\rangle = e^{-i(3\pi/2)S_y} W_\phi(\tau) |\psi_0\rangle, \quad (3)$$

where the W operator is defined by

$$W_\phi(\tau) = e^{iH(a)\tau} e^{-i\phi S_x} e^{-iH(a)\tau}, \quad (4)$$

with $S_x = \sum_{i,\alpha_i} s_{x\alpha_i}$ the x component of the *total* spin vector for the N -atom sample and $|\psi_0\rangle$ the fully x -polarized state. After the pulse sequence, the spin densities $n_{\uparrow z}(x)$ and $n_{\downarrow z}(x)$ are measured for a single cloud using two resonant absorption images, separated in time by $10 \mu\text{s}$. We define one repetition of this experimental sequence as a ‘‘single shot,’’ in Figs. 1(b) and 1(c). Inverse-Abel transformation of $[n_{\uparrow z}(x) - n_{\downarrow z}(x)]/2$ then measures $S_z(E_i, \phi) \equiv s_{zi}$, for a single shot, Fig. 1(c).

Now we connect the measured s_{zi} to information scrambling [10,13,19]. Consider a *single spin* labeled by α_i , with spin components $s_{x\alpha_i}, s_{y\alpha_i}, s_{z\alpha_i}$, interacting with the many-body system. It is straightforward to show [20]

$$C_{\alpha_i} \equiv \langle \psi_0 | [W_\phi(\tau), s_{x\alpha_i}]^2 | \psi_0 \rangle = \frac{1}{2} - \langle \psi_f | s_{z\alpha_i} | \psi_f \rangle. \quad (5)$$

As the many-body operator W_ϕ and the single spin operator $s_{x\alpha_i}$ initially commute, i.e., $[W_\phi(0), s_{x\alpha_i}] = 0$, a measurement of $\langle \psi_f | s_{z\alpha_i} | \psi_f \rangle$ determines how two initially commuting operators fail to commute at a later time, providing a measure of scrambling.

In the experiments, we measure the *collective* spin operators $s_{zi} = \sum_{\alpha_i} s_{z\alpha_i}$, where $\alpha_i \equiv (n_i, n_y, n_z)$ for fixed

n_i . The corresponding mean square commutator, averaged over the N_s spins with x energy E_i , is [20]

$$\frac{1}{N_s} \sum_{\alpha_i} C_{\alpha_i}(\phi, \tau) = \frac{1}{2} - \frac{1}{N_s} \sum_{\alpha_i} \langle \psi_f | s_{z\alpha_i} | \psi_f \rangle. \quad (6)$$

Further averaging Eq. (6) over atoms with energies within ΔE of $E_i \equiv E$, we replace the sum on the right-hand side by $S_z(E) \Delta E / [n(E) \Delta E]$, yielding the measured quantity

$$\mathcal{F}(E, \phi) \equiv \frac{1}{2} \frac{n_{\uparrow z}(E, \phi) - n_{\downarrow z}(E, \phi)}{n_{\uparrow z}(E, \phi) + n_{\downarrow z}(E, \phi)}. \quad (7)$$

Here, $n(E) = n_{\uparrow z}(E, \phi) + n_{\downarrow z}(E, \phi)$ is independent of ϕ and $\mathcal{F}(E, 0) = 1/2$.

We can extract information about the many-body coherence from Eq. (6), by writing the sum on the right-hand side as $\sum_m e^{im\phi} B_m$ [20]. Nonvanishing coefficients B_m correspond to coherence between states for which the x component S_x of the total angular momentum differs by m [17,20]. Since the sum is real, $B_{-m} = B_m^*$, we can expand Eq. (7) for the measured, energy-selected average in the form

$$\mathcal{F}(E, \phi) = B_0 + \sum_{m \geq 1} 2|B_m| \cos(m\phi + \varphi_m). \quad (8)$$

In fitting the data with Eq. (8), we restrict the range of m to 4. We find that the fits are not improved by further increase of m , consistent with the limited number of ϕ values measured in the experiments.

We measure spin density profiles $n_{\uparrow z, \downarrow z}(x, \phi)$ for a scattering length $a = 4.24a_0$. The data are averaged over 6 repetitions for each ϕ , with the ϕ values chosen in random order. We begin by finding the *total* number of atoms in each spin state $N_{\uparrow z, \downarrow z}(\phi) = \int dx n_{\uparrow z, \downarrow z}(x, \phi)$ for the protocol of Fig. 1(a), to find the total collective spin projection S_z versus rotation angle ϕ , *without* energy restriction. Figure 2(a) shows the normalized S_z data $F(\phi) = \frac{1}{2}(N_{\uparrow z} - N_{\downarrow z}) / (N_{\uparrow z} + N_{\downarrow z})$ (blue dots) and the fit of Eq. (8) (red solid curve)

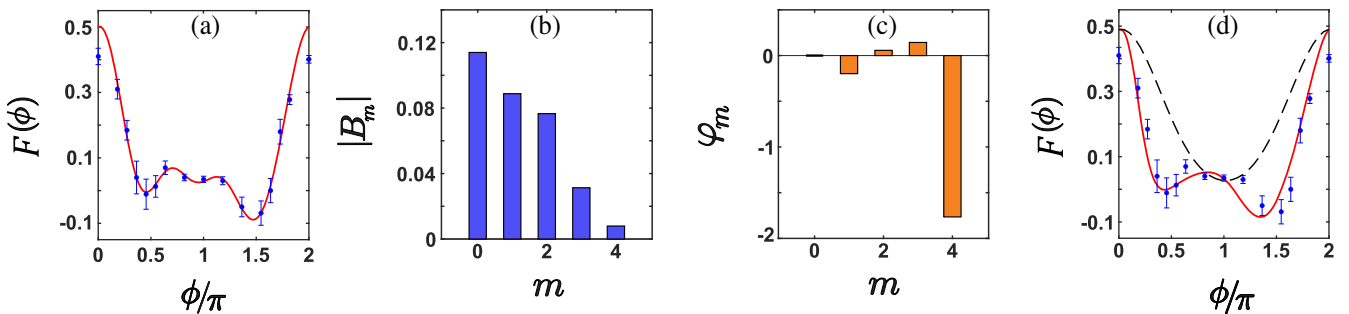


FIG. 2. Total collective spin projection S_z versus rotation angle ϕ without energy restriction. (a) $F(\phi) = \frac{1}{2}(N_{\uparrow z} - N_{\downarrow z}) / (N_{\uparrow z} + N_{\downarrow z})$ (blue dots) for a measured scattering length $a_{\text{meas}} = 4.24a_0$. The red solid curve is the fit of Eq. (8), which determines the magnitudes of the coherence coefficients $|B_m|$ (b) and corresponding phases φ_m (c). (d) Fit of the mean-field model of Ref. [4] to the data (blue dots) for a global detuning $\Delta = 0$ with $a = a_{\text{meas}}$ (black dashed curve) and with $a = 2.63a_{\text{meas}}$ (red solid curve).

curve), which determines the magnitude [Fig. 2(b)] and phase [Fig. 2(c)] of the average coherence coefficients B_m . We note that $F(0) \simeq F(2\pi) < 1/2$, the maximum for ideal conditions. This discrepancy arises from small variations in the phase shift of the final $\pi/2$ pulse, which is applied at a finite detuning as the magnetic field is ramped from B_2 back to its original value B_1 [20].

To check that the measurements are reasonable, we compare the ϕ -dependent data of Fig. 2 to a fit of our 1D mean-field model, which employs a calculated average transverse density \bar{n}_\perp to fit single-pulse spin-wave data with no free parameters [4]. The model, evaluated with a

global detuning $\Delta = 0$, is shown in Fig. 2(d). To fit the observed ϕ dependence (red solid curve), the model requires a scattering length $a_{\text{eff}} \equiv 2.63a_{\text{meas}}$, i.e., 2.63 times larger than the measured value $a_{\text{meas}} = 4.24a_0$, which yields the black dashed curve. The increased a_{eff} may occur because the measured coherence orders with $|m| > 1$ arise from interactions, favoring the largest couplings in a manner that is not predicted by our model.

Figure 3 shows the energy-resolved measurements $\mathcal{F}(E, \phi)$, obtained by inverse-Abel transformation of the same data. The top row shows significant variation in symmetry and structure as the energy is varied from $E = 0$

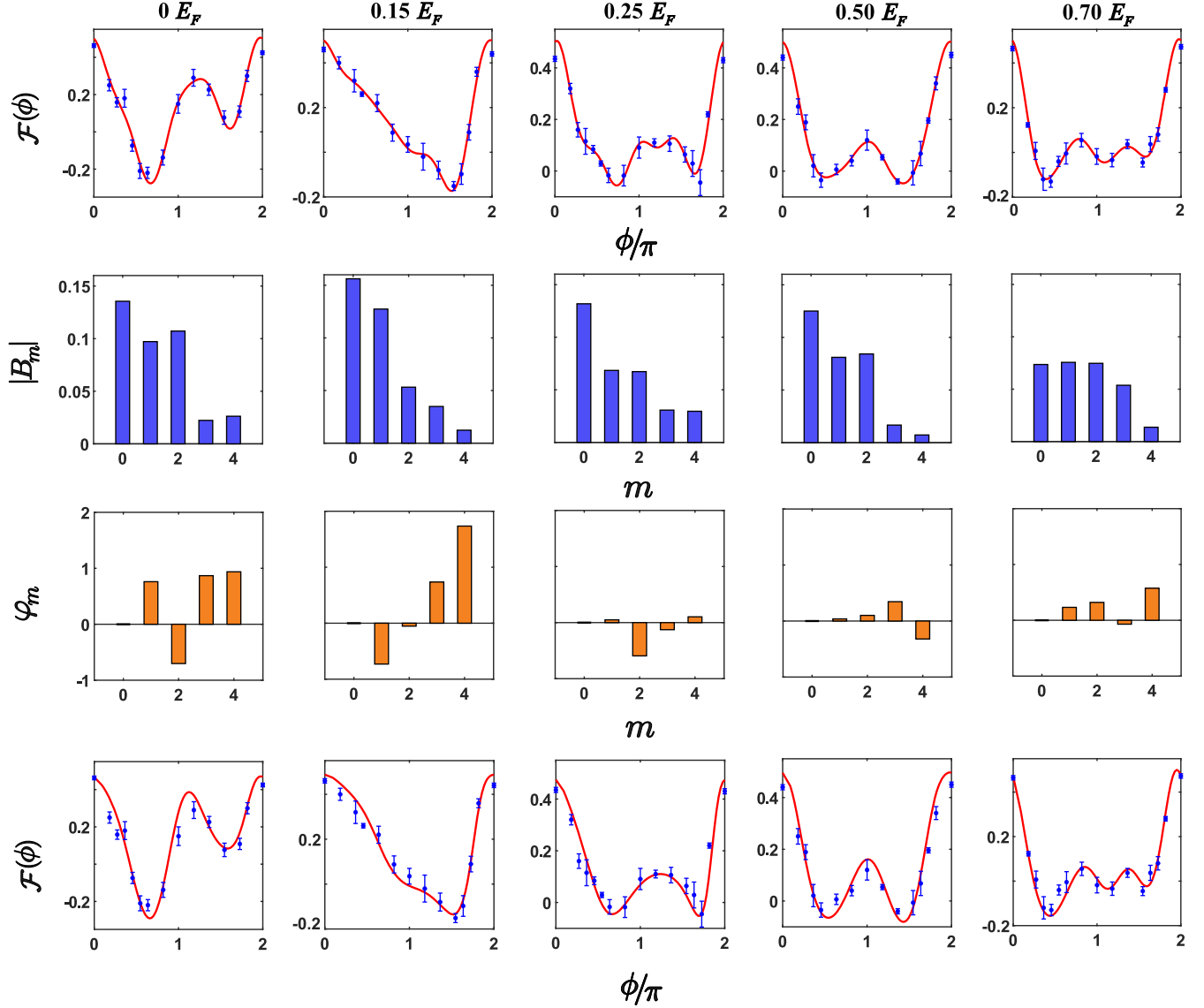


FIG. 3. Energy-resolved collective spin projection $S_z(E)$ versus rotation angle ϕ for spins of selected energies (left to right) $E/E_F = 0, 0.15, 0.25, 0.5, 0.7$. Here, $\mathcal{F}(\phi) = \frac{1}{2}[n_\uparrow(E) - n_\downarrow(E)]/[n_\uparrow(E) + n_\downarrow(E)]$. The top row shows the data (blue dots) for a measured scattering length $a = 4.24a_0$. The red solid curve is the fit of Eq. (8), which determines the magnitudes of the coherence coefficients $|B_m|$ (second row) and corresponding phases φ_m (third row). The bottom row shows the fits (red solid curves) of the mean-field model of Ref. [4] to the data (blue dots), using a scattering length 2.63 times the measured value and global detunings, ordered in energy, of $\Delta(\text{Hz}) = 0, 0.8, 0.65, -0.8, \text{ and } 0.15$.

to $E = 0.7E_F$. The red solid curves in the first row show the fit of Eq. (8), which yields the magnitudes of the coherence coefficients $|B_m|$ and the corresponding phases φ_m . In the last row, we compare the data to fits of the mean-field model [4]. Again, the model captures the complex ϕ -dependent shapes of the data with $a_{\text{eff}} = 2.63a_{\text{meas}}$, but a different detuning Δ is needed for each energy. This may be a consequence of averaging data over several detunings Δ , where each Δ rotates the direction of the ϕ -rotation axis by $\Delta\tau$ [26].

In summary, we have demonstrated a general method for measuring energy-resolved collective spin vectors in an energy-space lattice with effective long-range interactions. We have shown that an OTOC protocol can be implemented in this system and that many-body coherence can be measured in selected energy-space subsystems. Future measurement of time-dependent correlations between extensive subsets, $C_{ij}(t) \equiv \langle \psi_0 | s_{x_i}(t) s_{x_j}(t) | \psi_0 \rangle - \langle \psi_0 | s_{x_i}(t) | \psi_0 \rangle \langle \psi_0 | s_{x_j}(t) | \psi_0 \rangle$, enables a wide variety of protocols, extending correlation measurements in small numbers of trapped ions [27] to large quantum systems. For an initial x -polarized product state $|\psi_0\rangle$, $C_{ij}(t) = 0$ for noninteracting systems and for our mean-field model, so that $C_{ij}(t) \neq 0$ signifies beyond mean-field physics. As $C_{ij}(0) = 0$, a scrambling time [28,29] is determined by observing the evolution from the product state to a correlated state.

Primary support for this research is provided by the Air Force Office of Scientific Research (FA9550-16-1-0378) and the National Science Foundation (PHY-2006234). Additional support for the JETlab atom cooling group has been provided by the Physics Division of the Army Research Office (W911NF-14-1-0628) and by the Division of Materials Science and Engineering, the Office of Basic Energy Sciences, Office of Science, U.S. Department of Energy (DE-SC0008646).

*Corresponding author.
jethoma7@ncsu.edu

- [1] X. Du, Y. Zhang, J. Petricka, and J. E. Thomas, Controlling Spin Current in a Trapped Fermi Gas, *Phys. Rev. Lett.* **103**, 010401 (2009).
- [2] S. Smale, P. He, B. A. Olsen, K. G. Jackson, H. Sharum, S. Trotzky, J. Marino, A. M. Rey, and J. H. Thywissen, Observation of a transition between dynamical phases in a quantum degenerate Fermi gas, *Sci. Adv.* **5**, eaax1568 (2019).
- [3] X. Du, L. Luo, B. Clancy, and J. E. Thomas, Observation of Anomalous Spin Segregation in a Trapped Fermi Gas, *Phys. Rev. Lett.* **101**, 150401 (2008).
- [4] S. Pegahan, J. Kangara, I. Arakelyan, and J. E. Thomas, Spin-energy correlation in degenerate weakly interacting Fermi gases, *Phys. Rev. A* **99**, 063620 (2019).
- [5] F. Piéchon, J. N. Fuchs, and F. Laloë, Cumulative Identical Spin Rotation Effects in Collisionless Trapped Atomic Gases, *Phys. Rev. Lett.* **102**, 215301 (2009).
- [6] S. S. Natu and E. J. Mueller, Anomalous spin segregation in a weakly interacting two-component Fermi gas, *Phys. Rev. A* **79**, 051601 (2009).
- [7] C. Deutsch, F. Ramirez-Martinez, C. Lacroûte, F. Reinhard, T. Schneider, J. N. Fuchs, F. Piéchon, F. Laloë, J. Reichel, and P. Rosenbusch, Spin Self-Rephasing and Very Long Coherence Times in a Trapped Atomic Ensemble, *Phys. Rev. Lett.* **105**, 020401 (2010).
- [8] A. P. Koller, M. L. Wall, J. Mundinger, and A. M. Rey, Dynamics of Interacting Fermions in Spin-Dependent Potentials, *Phys. Rev. Lett.* **117**, 195302 (2016).
- [9] U. Ebling, A. Eckardt, and M. Lewenstein, Spin segregation via dynamically induced long-range interactions in a system of ultracold fermions, *Phys. Rev. A* **84**, 063607 (2011).
- [10] M. Gärtner, J. G. Bohnet, A. Safavi-Naini, M. L. Wall, J. J. Bollinger, and A. M. Rey, Measuring out-of-time-order correlations and multiple quantum spectra in a trapped-ion quantum magnet, *Nat. Phys.* **13**, 781 (2017).
- [11] G. Bentsen, T. Hashizume, A. S. Buyskikh, E. J. Davis, A. J. Daley, S. S. Gubser, and M. Schleier-Smith, Treelike Interactions and Fast Scrambling with Cold Atoms, *Phys. Rev. Lett.* **123**, 130601 (2019).
- [12] J. Eisert, M. Friesdorf, and C. Gogolin, Quantum many-body systems out of equilibrium, *Nat. Phys.* **11**, 124 (2015).
- [13] M. Schleier-Smith, Probing information scrambling, *Nat. Phys.* **13**, 724 (2017).
- [14] B. Swingle and N. Y. Yao, Seeing scrambled spins, *Physics* **10**, 82 (2017).
- [15] J. Li, R. Fan, H. Wang, B. Ye, B. Zeng, H. Zhai, X. Peng, and J. Du, Measuring Out-of-Time-Order Correlators on a Nuclear Magnetic Resonance Quantum Simulator, *Phys. Rev. X* **7**, 031011 (2017).
- [16] J. Marino and A. M. Rey, Cavity-QED simulator of slow and fast scrambling, *Phys. Rev. A* **99**, 051803 (2019).
- [17] M. Gärtner, P. Hauke, and A. M. Rey, Relating Out-of-Time-Order Correlations to Entanglement via Multiple-Quantum Coherences, *Phys. Rev. Lett.* **120**, 040402 (2018).
- [18] J. Baum, M. Munowitz, A. N. Garroway, and A. Pines, Multiple-quantum dynamics in solid state NMR, *J. Chem. Phys.* **83**, 2015 (1985).
- [19] R. J. Lewis-Swan, A. Safavi-Naini, J. J. Bollinger, and A. M. Rey, Unifying scrambling, thermalization and entanglement through measurement of fidelity out-of-time-order correlators in the Dicke model, *Nat. Commun.* **10**, 5007 (2019).
- [20] See Supplemental Material at <http://link.aps.org/supplemental/10.1103/PhysRevLett.126.070601> for a description of the experimental details and of the inverse Abel-transform method.
- [21] M. E. Gehm, S. L. Hemmer, K. M. O'Hara, and J. E. Thomas, Unitarity-limited elastic collision rate in a harmonically trapped Fermi gas, *Phys. Rev. A* **68**, 011603 (2003).
- [22] The number of atoms Δn_i at site i , i.e., in x mode E_i , summed over y, z transverse modes, is $\Delta n_i \simeq 3\Delta E_i N / E_F (1 - E_i / E_F)^2$. With $\Delta E_i = \hbar\omega_x$, $N = 6.5 \times 10^4$, and $E_i = E_F/2$, we find $\Delta n_i \simeq 74$.
- [23] Here, we employ a continuum approximation with $\bar{g} \equiv \int dn P(n) \int dn' P(n') g(n, n')$, in the notation of Ref. [4].

- [24] Nonzero matrix elements arise for transitions between states of relative motion with even x quantum number $2n$ and azimuthal quantum number $l=0$ [20]. For our trap, $\sqrt{\hbar/m\omega_x} \simeq 8.5 \mu\text{m}$ and $\nu_r/\nu_x = 27$. With $a = 4.24a_0$, $\langle 2n', m'_r | H' | 2n, m_r \rangle / \hbar\nu_x \simeq 3.2 \times 10^{-4} / (n'n)^{1/4}$, independent of the radial quantum numbers m_r, m'_r .
- [25] G. Pretzier, A new method for numerical Abel-inversion, *Z. Naturforsch. A* **46**, 639 (1991).
- [26] Note that a nonzero detuning Δ changes the effective axis of rotation to $\hat{e}_{x'} = \cos(\Delta\tau)\hat{e}_x + \sin(\Delta\tau)\hat{e}_y$ without changing the general ϕ -dependent structure of the OTOC [20].
- [27] P. Richerme, Z.-X. Gong, A. Lee, C. Senko, J. Smith, M. Foss-Feig, S. Michalakis, A. V. Gorshkov, and C. Monroe, Non-local propagation of correlations in quantum systems with long-range interactions, *Nature (London)* **511**, 198 (2014).
- [28] A. Y. Guo, M. C. Tran, A. M. Childs, A. V. Gorshkov, and Z.-X. Gong, Signaling and scrambling with strongly long-range interactions, *Phys. Rev. A* **102**, 010401 (2020).
- [29] J. Maldacena, S. H. Shenker, and D. Stanford, A bound on chaos, *J. High Energy Phys.* **08** (2016) 106.